Interplay between ballooning and peeling modes in simulations of the time evolution of edge localized modes

Thawatchai Onjun
Sirindhorn International Institute of Technology, Klong Luang, Pathumthani 12121, Thailand

Arnold H. Kritz and Glenn Bateman
Physics Department, Lehigh University, 16 Memorial Drive East, Bethlehem, Pennsylvania 18015

Vassili Parail and Howard R. Wilson
Euratom/UKAEA, Fusion Association, Culham Science Centre, Abingdon OX14 3DB, United Kingdom

Alex Dnestrovskij
Russian Science Centre Kurchatov Institute, Moscow, Russian Federation

(Received 19 March 2004; accepted 21 October 2004; published online 15 December 2004)

The time evolution of edge localized modes (ELMs) in the Joint European Torus tokamak [P. H. Rebut *et al.*, Nucl. Fusion **25**, 1011 (1985)] is investigated using the JETTO predictive modeling code [M. Erba *et al.*, Plasma Phys. Controlled Fusion **39**, 261 (1997)]. It is found that both pressure-driven ballooning and current-driven peeling modes can play a role in triggering the ELM crashes. In the simulations carried out, each large ELM consists of a sequence of quasicontinuous small ELM crashes. Each sequence of ELM crashes is separated from the next sequence by a relatively longer ELM-free period. The initial crash in each ELM sequence can be triggered either by a pressure-driven ballooning mode or by a current-driven peeling mode, while the subsequent crashes within that sequence are triggered by current-driven peeling modes, which are made more unstable by the reduction in the pressure gradient resulting from the initial crash. The HELENA and MISHKA ideal magnetohydrodynamic stability codes [A. B. Mikhailovskii *et al.*, Plasma Phys. Rep. **23**, 713 (1997)] are used to validate the stability criteria used in the JETTO simulations. This stability analysis includes infinite-*n* ideal ballooning, finite-*n* ballooning, and low-*n* kink/peeling modes. © *2005 American Institute of Physics*. [DOI: 10.1063/1.1832600]

I. INTRODUCTION

The improved confinement regime in tokamaks known as the high confinement mode (H mode) is often perturbed by the onset of quasiperiodic bursts of magnetohydrodynamic (MHD) activity and D_α emission at the edge of the plasma known as edge localized modes (ELMs). Each ELM crash results in a rapid loss of particles and energy from the edge of the plasma, which reduces the average global energy content by up to 10%.[1] Furthermore, these transient bursts of energy and particles into the scrape-off layer produce high peak heat loads on the divertor plates. On the other hand, the ELMs play an important role in removing excessive heat and particles, as well as impurities from the region near the separatrix. It is generally accepted that ELMs control the plasma parameters at the top of the pedestal in H-mode plasmas. The pedestal, in turn, has a strong influence on the energy confinement of tokamak plasmas due to the observed stiffness in the ion and electron temperatures.[2] Consequently, ELMs are likely to affect the performance in burning plasma experiments such as the International Thermonuclear Experimental Reactor (ITER),[3] and it is important to understand the physical mechanisms that trigger ELM crashes.

As the plasma makes the transition from the low confinement mode (L mode) to the H mode, a steep pressure gradient, called the pedestal, develops in a region at the edge of the plasma. This steep pressure gradient results in an increase in the bootstrap current within the pedestal. The increase in the edge pressure gradient and in the edge current density leads to a destabilization of MHD modes, which results in a loss of plasma energy and particles to the wall. The destabilization is believed to be caused either by a pressure-driven ballooning mode[4,5] or by a current-driven peeling mode.[1,6–9] The pressure-driven ballooning mode becomes unstable when the pressure gradient exceeds a critical pressure gradient, while the current-driven peeling mode occurs when the current density exceeds a critical current density. The effects of ELMs in simulations of H-mode plasmas have been considered in a number of papers.[10–14] In core-edge simulations carried out using the JETTO code[10–12] and the ASTRA code,[13] only the pressure-driven ballooning mode was considered as an ELM trigger. However, it was found in Ref. 14 that a current-driven peeling mode can also play a role in triggering the ELM crashes that limit the pressure at the top of the pedestal. JETTO simulations indicate that the interaction of physical processes involving ELMs triggered by a current-driven peeling mode cause the pressure at the top of the pedestal to increase with heating power as observed in experiment.[14]

In this paper, a new version of the JETTO code is used, which includes criteria for both pressure-driven ballooning modes and current-driven peeling modes to trigger the onset of ELM crashes. The current-driven peeling criterion is taken from an analytical formula developed in Ref. 1. The instability that results in the crash depends on which mode reaches

its stability limit first. Simulations are carried out for discharges that have core and edge parameters similar to those obtained in Joint European Torus (JET) discharges. It is found in the simulations that a sequence of ELM crashes rather than a single ELM crash can occur in some circumstances. This sequence is caused by an interaction between different modes during an ELM crash. The ELM model explored in this paper is similar to the ELM models proposed in Refs. 15 and 16.

The MHD equilibrium and stability analyses codes, HELENA and MISHKA,[17] are used to evaluate the edge stability of the plasma just before an ELM crash in order to confirm the validity of the simplified stability criteria used to trigger ELMs in the JETTO simulations. The instabilities included are the infinite-n ideal ballooning, the finite-n ballooning, and the low-n kink/peeling modes. JETTO simulates the time evolution of the main plasma parameters both during and between ELMs.

ELM crashes are simulated in the JETTO code by transiently increasing the thermal and particle diffusivities near the edge of the plasma. This model is not meant to reproduce the details of each ELM crash. A nonlinear extended MHD simulation or a fully kinetic first principles simulation is needed to properly reproduce the details of each ELM crash. Instead, the diffusive model used in the JETTO code is only meant to compute the changes in the shapes of the plasma profiles near the edge of the plasma from the time before an ELM crash to the time after an ELM crash. The MHD instability models in the JETTO code are only used to trigger the ELM crashes in the simulations. The nonlinear development of the MHD instability that is believed to cause an ELM crash is not considered in this model. Hence, the ELM crash model used in the JETTO code should only be considered as a technique for changing the plasma profiles in the way that an ELM crash changes those profiles in the experiments. The goal in carrying out the JETTO simulations and the associated MHD stability investigation is to obtain a better understanding of the driving mechanism for ELM crashes during the course of the discharge.

This paper is organized as follows. The codes used in the study, JETTO, HELENA, and MISHKA, are briefly described in Sec. II. The criteria for triggering ELM crashes in the JETTO simulation are given in Sec. III. Simulation results and a stability analyses are presented in Sec. IV, followed by conclusions in Sec. V.

II. CODES USED IN THE STUDY

In this paper, simulations are carried out using predictive JETTO code, while the MHD stability analyses involve use of the HELENA and MISHKA codes. These codes are described in this section.

A. The JETTO code

The JETTO 1.5D transport code[18] is used to evolve the plasma current, temperature, and density profiles in both the core and pedestal regions. The core transport is calculated using the mixed Bohm/gyro-Bohm model,[19] which includes both thermal and particle transport. The interaction between the recycled neutrals and the edge plasma is computed using the FRANTIC module in the JETTO code. The pedestal in the JETTO simulation is produced by assuming that the turbulent transport is suppressed in the region between the top of the pedestal and the separatrix. For simplicity, all the diagonal elements of the transport matrix within the pedestal are taken to be the ion neoclassical thermal conductivity, calculated at the top of the pedestal using the NCLASS model.[20] This simplification is motivated by the fact that the pedestal width is usually of the order of the ion orbit width (or banana width), which implies limited variation of the neoclassical transport across the barrier. A fixed pedestal width of 3 cm is assumed in the simulations carried out in this paper.

Edge boundary conditions are imposed at the separatrix for the ion density and for the electron and ion temperatures. The electron and ion temperature at the separatrix are taken to be 20 eV in most of the simulations, and the ion density at the separatrix is assumed to be 1×10^{19} m^{-3} in all simulations. The values of the temperatures at the separatrix are varied in Sec. IV in order to test the sensitivity of the simulations to the separatrix temperature. Note that the ion and electron temperature and the ion density at the separatrix are kept constant throughout each simulation. In experiments, the ion and electron temperature and the ion density at the separatrix do change over time, especially during an ELM crash. Unfortunately, the JETTO code does not take this effect into an account. Although the constant values of the electron and ion temperature at the separatrix influence the time evolution of the ELMs (for example, the duration of the ELM crashes), these values do not affect the overall energy confinement.

B. MHD stability codes

To justify the simplified models used to trigger ELM crashes in the JETTO code, MHD stability analyses are carried out using the HELENA and MISHKA codes.[17] The HELENA code is used to refine the equilibrium and to compute the stability of infinite-n ideal ballooning modes. The HELENA code takes plasma profiles and equilibrium information, generated by JETTO and produces an equilibrium with the higher resolution that is needed for the MISHKA code. MISHKA is then used to evaluate the stability criteria for finite-n ballooning and low-n kink/peeling modes. In this study, the MISHKA stability analysis is carried out for modes with toroidal mode number $n=1$–14. The version of the MISHKA code used in this paper is based on the ideal MHD model.

III. MODELS FOR TRIGGERING ELMS

In the JETTO simulations, the reduced transport within the pedestal region results in the development of a steep pressure gradient, which causes an increase in the bootstrap current within the pedestal. The increase of edge pressure gradient, and the resulting increase in the edge current density, leads to a destabilization of either a pressure-driven ballooning mode or a current-driven peeling mode. The result-

ing MHD instability triggers an ELM crash with an associated loss of plasma energy and particles to the wall.

The criterion used in the JETTO code for an ELM crash triggered by a pressure-driven ballooning mode is that the normalized pressure gradient α at any location within the pedestal region exceeds a critical value α_c. That is

$$\alpha \equiv -\frac{2\mu_0 q^2}{\epsilon B_T^2}\frac{\partial p}{\partial \rho} > \alpha_c, \tag{1}$$

where μ_0 is the permeability of free space, q is the safety factor, ϵ is the inverse aspect ratio, B_T is the toroidal magnetic field, and $\partial_p/\partial\rho$ is the pressure gradient. Note that α_c is a number determined as a result of stability analyses carried out using the HELENA and MISHKA codes.

The criterion for an ELM crash triggered by a current-driven peeling mode is that the current density anywhere within the pedestal exceeds a critical current density. This critical current density model is based on an analytical expression developed in Ref. 1. For axisymmetric toroidal geometry, the current-driven peeling instability condition is

$$\sqrt{1-4D_M} + C_{\text{vac}} < 1 + \frac{1}{\pi q'}\oint \frac{\mu_0 J_{\parallel} B_T}{R^2 B_p^3} dl, \tag{2}$$

where D_M is the Mercier coefficient, which is proportional to pressure gradient; C_{vac} is a parameter related to the vacuum energy, which is taken to be 0.2 for the baseline simulations in this study; q' is the derivative of the safety factor with respect to the poloidal flux; μ_0 is the vacuum magnetic permeability; $J_{\parallel}$ is the current density parallel to the magnetic field **B**; R is the major radius; B_p is the poloidal magnetic field; and dl is the poloidal arc length element for the integral around a flux surface.

When the condition for an ELM crash is satisfied either by the pressure-driven ballooning mode criterion [Eq. (1)] or by the current-driven peeling mode criterion [Eq. (2)], an ELM crash in the JETTO simulation is produced as follows: The diagonal transport coefficients for electron and ion thermal transport within the pedestal are temporarily increased to 300 times the ion neoclassical diffusivity at the top of the pedestal, while the particle transport coefficients in the pedestal are increased to 100 times the ion neoclassical diffusivity at the top of the pedestal. This choice for the transport multiplication factors was made in order to reproduce in the simulations the values of the JET experimental ELM frequency and the plasma energy content presented in Refs. 12 and 14. The increased levels of transport are maintained for a time interval $\tau_{\text{ELM}}=0.4$ ms, which is of the order of a typical type-I ELM crash duration in JET. The large increase of the transport within the pedestal leads to a loss of particles and energy, comparable to the loss during an ELM crash in experiment.

The ELM transport model, described above, has a number of *ad hoc* parameters that determine both the ELM amplitude and its repetition rate. This model, which has been tested against a wide range of JET data, leads to the following conclusions: The ELM amplitude (taken as the ratio of the energy loss during an ELM crash to the average plasma energy) scales linearly with the parameter $H_{\text{particle,thermal}}$ $\propto A_{\text{particle,thermal}}\,\tau_{\text{ELM}}$, and the ELM frequency scales inversely proportional to H. In reality, it is believed that both the ELM amplitude and its duration are controlled by nonlinear MHD phenomena. The values of $A_{\text{particle,thermal}}$ and τ_{ELM} are adjusted in order to bring the simulation results into closer agreement with experimental data, since a more detailed model for ELM crashes is not yet fully developed. It is found that the time averaged total plasma energy content does not depend sensitively on the parameter $H_{\text{particle,thermal}}$. Instead, the thermal energy confinement time is almost entirely controlled by the core transport (which in turn depends on plasma parameters at the top of the H-mode pedestal). This is a result of the profile stiffness associated with the core transport.[21–24]

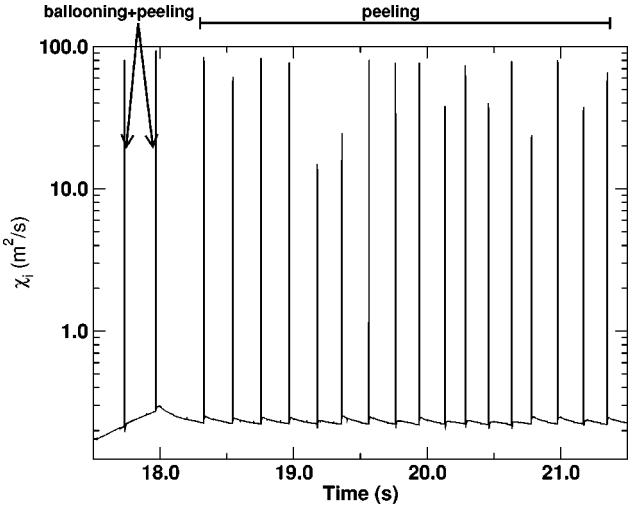

FIG. 1. The time history of the ion diffusivity at a location corresponding to the top of the pedestal is plotted between 17.5 and 21.5 s. The rapid increase in the ion diffusivity at the top of the pedestal indicates an ELM crash sequence in the JETTO simulation. The first two sequences of ELM crashes include ELMs that are triggered by a combination of ballooning and peeling modes, while the remaining 17 ELM crash sequences that occur between 18.0 and 22.5 s contain ELMs triggered only by the peeling mode.

IV. RESULTS AND DISCUSSION

The simulation is carried out for the plasma parameters similar to those of JET discharge 44013;[25] i.e., major radius $R=2.91$ m, minor radius $\alpha=0.94$ m toroidal magnetic field $B_T=2.76$ T plasma current $I_p=2.57$ MA, elongation $\kappa=1.75$, and triangularity $\delta=0.22$. During the quasistationary H-mode phase of the discharge, the line averaged electron density is 5.82×10^{19} m^{-3}, the neutral beam injected heating power is 13.9 MW, and Z_{eff} is 2.14.

A. JETTO simulation

Figure 1 shows the time history of the ion diffusivity at the radius that corresponds to the top of the pedestal. The rapid increase of the ion diffusivity at this radius indicates an ELM crash in the JETTO simulation. It is found in the simulation that what appear to be individual ELM crashes in Fig. 1 are, in fact, sequences of quasicontinuous small ELM crashes separated by relatively longer ELM-free periods. In the sequence of ELM crashes at 17.73 s, for example, the

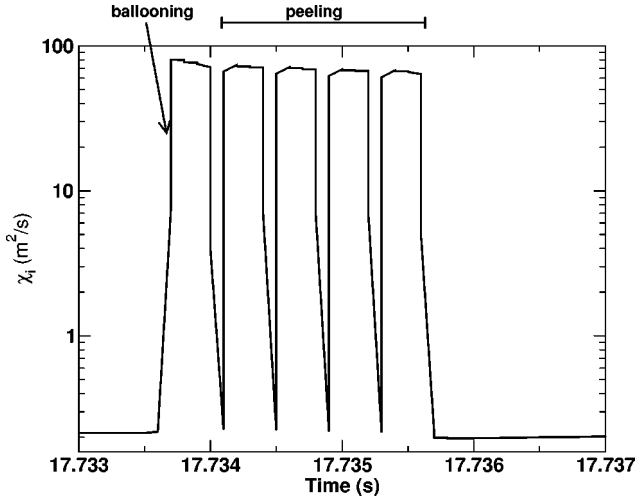

FIG. 2. The ion diffusivity at the top of the pedestal is plotted as a function of time for the first sequence of ELM crashes shown in Fig. 1. In this sequence of five ELM crashes, the first ELM crash is triggered by a pressure-driven ballooning mode while the subsequent ELM crashes in this sequence are triggered by a current-driven peeling mode.

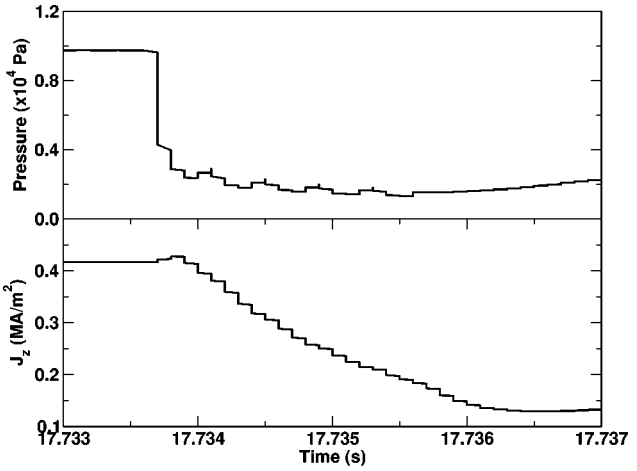

FIG. 3. The simulated plasma pressure and plasma current density J_z at the normalized radius $\rho=0.97$ are plotted as a function of time during the sequence of ELM crashes shown in Fig. 2.

first ELM crash is triggered by a pressure-driven ballooning mode while the remaining ELM crashes in that sequence are triggered by current-driven peeling modes. The details of this sequence of ELM crashes will be discussed below. A similar sequence of ELM crashes occurs at 17.97 s. On the other hand, ELM crashes in the remaining ELM sequences shown in Fig. 1 are triggered only by current-driven peeling modes.

In Fig. 2, the ion diffusivity at the top of the pedestal during the first sequence of ELM crashes in Fig. 1 is plotted as a function of time using an expanded time scale. It can be seen that this sequence of ELM crashes consists of five individual ELM crashes, each 0.4 ms long (as is prescribed by the JETTO code). The first ELM crash in this sequence is triggered by a pressure-driven ballooning mode, that is as a consequence of the condition given in Eq. (1), while the rest of the ELM crashes are triggered by current-driven peeling modes, that is as a consequence of the condition given in Eq. (2).

The sequence of ELM crashes can be understood as follows: After the first ELM crash occurs, the edge pressure gradient decreases significantly, which results in a lower value of D_m (which is proportional to the pressure gradient) in Eq. (2). The decrease in the value of D_m results in a lower value for the critical current density needed to drive a peeling instability [$J_\parallel$ on the right-hand side of Eq. (2)]. The model for the ELM crash used in the study is diffusive, in that transport within the pedestal is rapidly increased to a high value during an ELM crash. This does not directly affect neoclassical plasma resistivity (apart from the temperature dependence), and, as a result, the current density in the pedestal is decreased only slightly during the first ELM crash of the sequence. Since the value of D_m, which is proportional to the pressure gradient, is significantly reduced during the first ELM crash, the current density that remains in the pedestal region is still large enough to trigger the peeling instability, which leads to subsequent ELM crashes. Gradually, the pedestal current density is reduced by resistive diffusion until the current-driven peeling mode criterion given in Eq. (2) is no longer satisfied, and the sequence of ELM crashes comes to an end. The observation about the trigger for ELM crashes that the pressure-driven ballooning mode is unstable first and then the current-driven peeling mode becomes unstable is similar to the ELM model proposed in Refs. 15 and 16.

Figure 3 shows the time history of pressure and current density at normalized radius $\rho=0.97$ during the ELM crash sequence shown in Fig. 2. Note that the normalized radius $\rho=0.97$ is located in the middle of the pedestal region. It can be seen that the pressure within the pedestal decreases rapidly during the first ELM crash, while the current density in the middle of the pedestal at $\rho=0.97$ decreases gradually during the sequence of ELM crashes. In Fig. 4, the radial profiles are plotted from $\rho=0.50$ to the edge of the plasma for the plasma pressure and the current density at several times during the initial ELM crash sequence shown in Figs. 2 and 3. It can be seen that at $t=17.7338$ s, which is the time just after the first ELM crash in that sequence, the pressure decreases significantly in the region between $\rho=0.85$ and $\rho=1.00$ ($\rho=1.00$ is at the separatrix) compared with the pressure at $t=17.7334$ s, which is the time just before the first ELM crash. In comparison, the edge current density at $t=17.7338$ s decreases only slightly compared with the current density at $t=17.7334$ s. After five consecutive ELM crashes, the edge current density decreases sufficiently so that the current-driven peeling modes are no longer unstable at 17.7359 s. This sequence of ELM crashes results in a total ELM crash duration of 2 ms. Note that at the time just before the first ELM crash of the sequence, the current density in the core region near the top of the pedestal is close to zero. This low value of current density is caused by inductive effects as the current density is driven in the steep gradient region of the pedestal and the total plasma current is conserved in the simulation. Since experimental measurements do not provide detailed measurements of the evolution of the current density within the pedestal, it is not possible, at

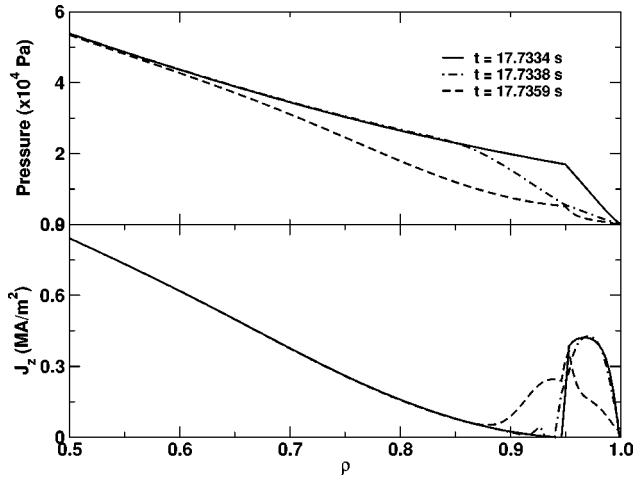

FIG. 4. Plasma pressure and current density profiles are plotted at three times during the first sequence of ELM crashes shown in Fig. 2. The solid line shows the profiles at $t=17.7334$ s, just before the first ELM crash of the sequence. The chained line shows the profiles at $t=17.7338$ s, just after the first ELM crash. The dashed line shows the profiles at $t=17.7359$ s, after the end of the sequence of the five ELM crashes. Note that at the time just before the first ELM crash of the sequence, the current density in the core region near the top of the pedestal is close to zero. This low value of current density is caused by inductive effects as the current density is driven in the steep gradient region of the pedestal and the total plasma current is conserved in the simulation.

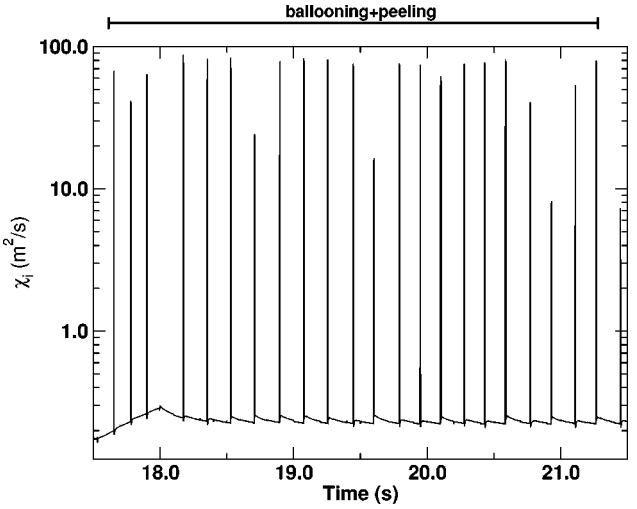

FIG. 5. The time history of the ion diffusivity at the top of the pedestal is plotted between 17.5 and 21.5 s. This simulation is carried with the pressure gradient limit that is 13% lower than the pressure gradient limit used in Fig. 1. All of the 23 sequences of ELM crashes in this simulation are triggered by a combination of ballooning and peeling modes.

present, to use direct comparisons between experimental data and the current density in the simulations to improve the ELM model.

The results shown in Figs. 2–4 can be interpreted in the following way: The compound ELM crash model removes pressure gradient and current density from the pedestal until the pressure-driven ballooning modes and the current-driven peeling modes are all stabilized. The pressure gradient and current density then rebuild in the pedestal until either a ballooning mode or a peeling mode are destabilized, which triggers the next ELM crash. Since, the pressure gradient rebuilds more rapidly than the current density, the pressure gradient stabilizes the peeling mode while the current density rebuilds.

This compound ELM crash model produces a reasonable upper bound on the pressure gradient and current density that remains in the pedestal after each ELM crash. If the remaining current density were higher than predicted by this model, then another ELM crash would be immediately triggered by a peeling mode until the current density were reduced to the level predicted by the model. If, in reality, the remaining current density were lower than the small level predicted by this model, then the result for the ELM frequency would be about the same, since most of the current density has to rebuild before triggering the next ELM crash in any event. The same argument applies to the pressure gradient that remains after an ELM crash. It takes about the same amount of time for the pressure gradient to rebuild from a small value that it would take to rebuild from a very small value. Hence, for the purpose of predicting the ELM frequency, the model predicts approximately the correct profiles after each ELM crash, without having to work through all of the details of the nonlinear evolution of the ELM crash.

The duration of the ELM crash predicted by this model (e.g., the 2 ms duration shown in Fig. 2) is longer than the 0.4 ms that is typical of the ELM crash duration in experiments, but is much smaller than the time between ELM crashes, as can be seen in Fig. 1, for example. The objective of this study is to demonstrate that either peeling modes or ballooning modes can trigger ELMs in the simulations. A more sophisticated model would be needed to predict the observed duration of each ELM crash.

B. Sensitivity of ELM history to variations in the conditions for triggering ELMs and to the value of the separatrix temperature

1. Variation of α_c

As mentioned in Sec. III, the value of the critical pressure gradient α_c in the JETTO code is a prescribed number that is calibrated by stability analyses carried out using the HELENA and MISHKA stability codes. It is found in the JETTO simulations that the choice of the pressure gradient limit α_c influences the time evolution of ELMs.

A simulation is carried out in which α_c is 13% lower than the value of α_c used to obtain the results presented in Fig. 1. The time history of the ion diffusivity at the radius that corresponds to the top of the pedestal is shown in Fig. 5. It is found that the frequency of the ELM sequences increases as α_c decreases. The frequency of the ELM sequences in Fig. 1 is 4.75 Hz while the frequency of the ELM sequences shown in Fig. 5 (the simulation result for which α_c is decreased) is 5.75 Hz. In all the sequences of ELM crashes shown in Fig. 5, the initial ELM of each sequence is triggered by a pressure-driven ballooning mode while the remaining ELMs in that sequence are triggered by current-driven peeling modes. This is in contrast to the results of the simulation presented in Fig. 1 where after the second ELM sequence all the subsequent ELMs are triggered only by current-driven peeling modes.

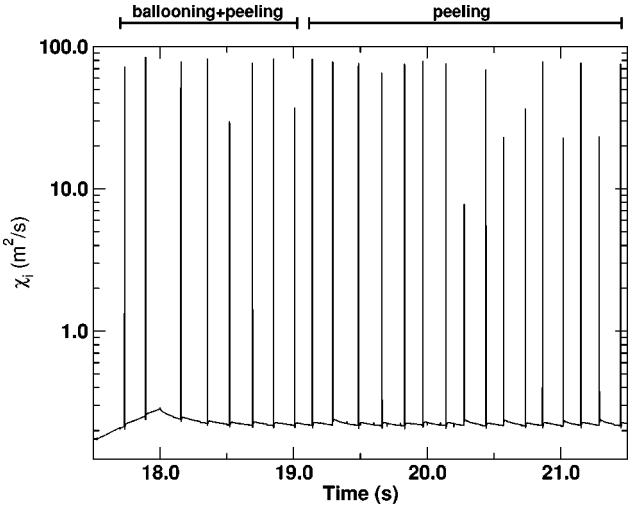

FIG. 6. The time history of the ion diffusivity at the top of the pedestal is plotted between 17.5 and 21.5 s. This simulation is carried with $C_{vac}=1.0$. The first eight sequences of ELM crashes are triggered by a combination of ballooning and peeling modes, while the rest of the 16 sequences of ELM crashes are triggered by peeling modes only.

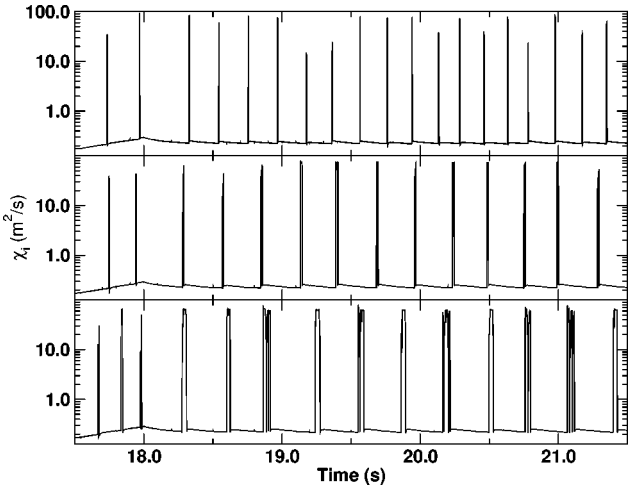

FIG. 7. Ion diffusivity at the top of the pedestal as a function of time from a simulation using $T_{sep}=20$ eV in the top panel, $T_{sep}=100$ eV in the middle panel, and $T_{sep}=200$ eV in the bottom panel.

2. Variation of parameter C_{vac}

The parameter C_{vac} in Eq. (2), for an ELM crash triggered by a current-driven peeling mode, is related to the vacuum energy. It is found in the JETTO simulations that the choice of the parameter C_{vac} influences the time evolution of ELMs. In this subsection, the effect of increasing the value of this parameter is examined.

Figure 6 shows the time history of the ion diffusivity at the radius that corresponds to the top of the pedestal for the simulation using $C_{vac}=1.0$, compared with using $C_{vac}=0.2$ in the other simulation results presented in this paper. All other parameters, including α_c, are kept the same as in the baseline simulation used to obtain the result presented in Fig. 1. It is found that as the value of the parameter C_{vac} increases, the ELM frequency increases. The ELM frequency increases from 4.75 Hz in Fig. 1 ($C_{vac}=0.2$) to 6.00 Hz in Fig. 6 ($C_{vac}=1.0$). It is also found that the number of ELM sequences that are triggered by a combination of pressure-driven ballooning and current-driven peeling modes is increased from two sequences in Fig. 1 ($C_{vac}=0.2$) to eight sequences in Fig. 6 ($C_{vac}=1.0$).

The duration of longest ELM sequence becomes shorter as the parameter C_{vac} is increased. In the simulation with $C_{vac}=0.2$, the duration of the longest ELM sequence is 3.6 ms and consists of nine small ELM crashes. In contrast, in the simulation with $C_{vac}=1.0$, the duration of the longest ELM sequence is 1.6 ms and consists of four small ELM crashes. The shorter duration of the ELM sequence can be explained by the fact that a higher edge current density is required to destabilize a current-driven peeling mode as the parameter C_{vac} is increased. As a result, less edge current needs to be removed to stabilize the current-driven peeling modes during each ELM crash sequence. Furthermore, since the ELM duration becomes shorter, the energy loss during each ELM sequence is reduced, resulting in less time needed to recover before the next ELM sequence. Consequently, the ELM frequency increases with the increase in the value of the parameter C_{vac}.

3. Variation of T_{sep}

It is found in the JETTO simulations that the temperature at the separatrix T_{sep} has an influence on the time evolution of ELMs. The electron temperature $T_{e,sep}$, ion temperature $T_{i,sep}$, and ion density at the separatrix are imposed as boundary conditions in the JETTO simulations. The electron and ion temperature at the separatrix are set equal to each other in all of the simulations ($T_{e,sep}=T_{i,sep}=T_{sep}$). In Fig. 7, the time history of the ion diffusivity at the top of the pedestal is plotted for simulations using T_{sep} of 20 eV (top panel), 100 eV (middle panel), and 200 eV (bottom panel). It can be seen that the duration of the ELM crash sequence in the simulation using $T_{sep}=20$ eV is briefer than the duration using $T_{sep}=200$ eV. Also, the frequency of the sequence of ELM crashes decreases from 4.75 Hz in the simulation using $T_{sep}=20$ eV to 3.50 Hz in simulation using $T_{sep}=200$ eV.

As noted in Sec. III, an ELM crash in the JETTO code is implemented by increasing the transport within the pedestal (300 times for thermal and 100 times for particle transport) during the crash. The increased transport results in the rapid loss of temperature and particles, but not in the rapid loss of edge current density. In the JETTO code, the reduction of the current density occurs as a result of the resistive redistribution of the current density at the edge of the plasma. A higher edge resistivity, which is a consequence of a lower temperature, results in a more rapid reduction of the edge current density when an ELM crash occurs. The neoclassical expression for electrical resistivity, used in the JETTO code, is inversely proportional to the electron temperature. As a result, the edge current density changes more slowly during an ELM crash in a simulation with a high value of T_{sep} than that in a simulation with a low value of T_{sep}. It is seen in Fig. 7 that the duration of each ELM crash decreases and the frequency of ELMs increases as the temperature at the separa-

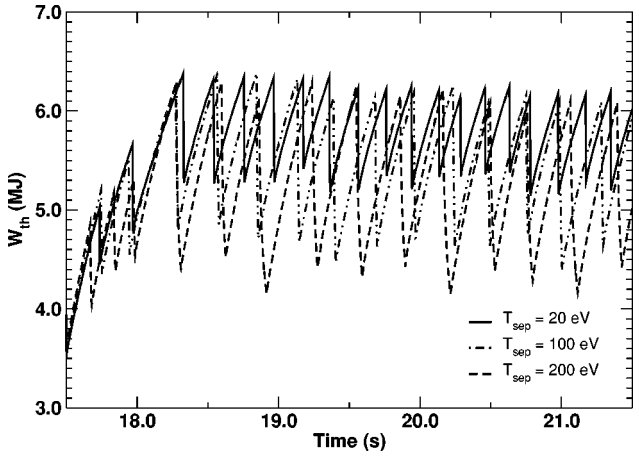

FIG. 8. Thermal energy content W_{th} is plotted as a function of time from the simulations using $T_{sep}=20$ eV, $T_{sep}=100$ eV, and $T_{sep}=200$ eV. The peak values of thermal energy content before each sequence of ELM crashes are nearly the same in all the simulations. However, the minimum values of thermal energy content after each sequence of ELM crashes are different in the different simulations. This is a consequence of the longer duration of the ELM crash sequences in the simulations with higher T_{sep}.

trix is reduced. However, even with the low value of T_{sep} ($T_{sep}=20$ eV), the duration of ELM crashes is still higher than a typical experimentally observed ELM duration, which is usually less than 1 ms. Consequently, it would appear that an ELM crash triggered by a current-driven peeling mode cannot be adequately described by a simple diffusive model for the redistribution of edge density and temperatures. To improve the agreement with the experimental results, either anomalous current diffusivity or dynamo effects are required. The discussion of those effects remain for future work. It is worth noting though that even with the present model, it is found that the temperature and density at the top of the pedestal before each composite ELM crash, as well as the thermal energy content and the global plasma confinement time, are nearly independent of T_{sep}. The thermal energy content W_{th} is shown as a function of time in Fig. 8 for simulations with $T_{sep}=20$, 100, and 200 eV.

C. Stability analysis

In order to check the validity of the analytical ballooning stability criterion used in JETTO, the code is linked with the HELENA and MISHKA MHD stability analysis codes. The HELENA code uses, at a time just prior to an ELM crash, the self-consistent equilibrium produced by the JETTO code—that is, the pressure gradient and the current density profiles together with the corresponding magnetic configuration. The HELENA code then reconstructs the equilibrium on a finer grid in order to provide the resolution required for the stability analysis. This refined equilibrium is used in the HELENA code to generate an infinite-n ballooning stability s-α diagram. Furthermore, a version of the MISHKA code, which is based on the ideal MHD model without dissipation or flow shear, is used to evaluate the stability criteria for finite-n ballooning and low-n kink/peeling modes. In this study, the stability analysis is carried out in the MISHKA code for toroidal mode numbers in the range of $n=1$–14.

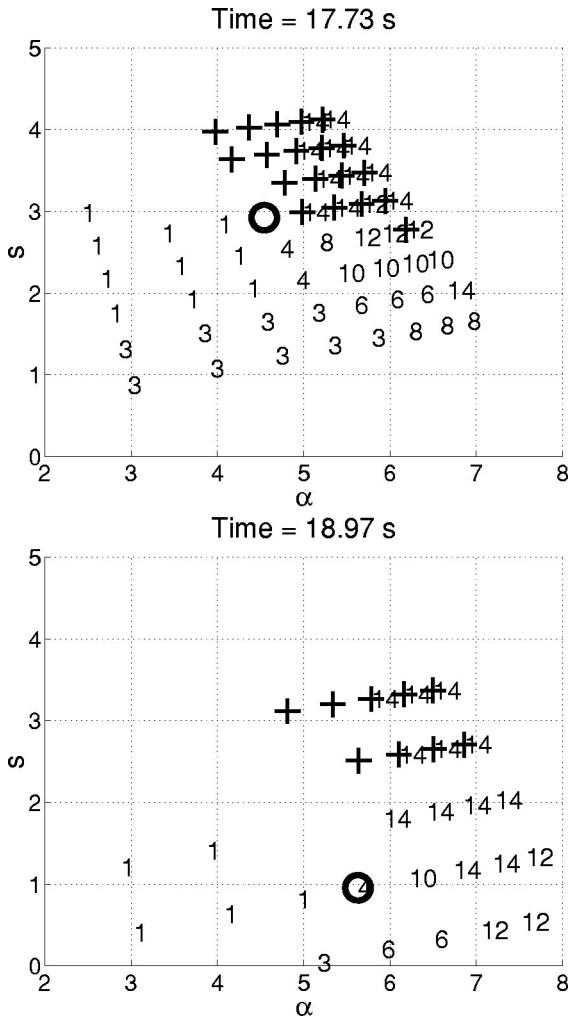

FIG. 9. Stability results obtained using the HELENA and MISHKA codes are plotted for the flux surface at normalized radius $\rho=0.95$ on an s-α stability diagram just before the first ELM crash of the sequence that occurs at $t=17.73$ s (top panel) and at $t=18.97$ s (bottom panel). Crosses mark the region that is unstable to infinite-n ideal ballooning modes. The numbers indicate the most unstable finite-n ballooning and low-n kink/peeling modes at each location on the s-α plane. All of the modes are stable in the region without numbers or crosses.

The results of the stability analyses carried out with the HELENA and MISHKA codes are presented in Fig. 9. In the top panel, the s-α stability diagram is shown at the time just prior to the first ELM crash in the first sequence of ELM crashes that appears in Fig. 1 ($t=17.73$ s). In the bottom panel, the s-α stability diagram is shown at the time just prior to the first ELM crash in the sixth sequence of ELM crashes that appears in Fig. 1 ($t=18.97$ s). In each panel, the stability s-α diagram is plotted for the flux surface at normalized radius $\rho=0.95$. The circle symbol represents the location of the operational point, given by the JETTO code, for the pressure gradient and magnetic shear at that flux surface. The region of instability associated with the infinite-n ideal ballooning modes is indicated with crosses, while the numbers on these plots indicate the toroidal mode number of the most unstable finite-n ballooning and low-n kink/peeling modes at each location on the s-α plane.

It can be seen that the pedestal pressure gradient at t

$=17.73$ s is close to the region of the infinite-n ballooning mode (indicated by crosses), but also not far from the region of low-n kink mode. Note that it is found in the JETTO simulation that the first ELM crash of the sequence of ELM at $t=17.73$ s is triggered by a pressure-driven ballooning mode. It can also be seen that the ELM at $t=18.97$ s (just before the sixth sequence of ELM crashes in Fig. 1) is triggered by a low-n kink mode ($n=4$). This result is also consistent with the JETTO simulation described in Sec. IV A in that the first ELM crash of the sequence of ELM at $t=18.97$ s is triggered by a current-driven peeling mode.

V. CONCLUSION

It is found in the JETTO simulations that the stability criteria based on pressure-driven ballooning modes and current-driven peeling modes both play a role in triggering ELM crashes. Early in the discharge, ELMs tend to be triggered by ballooning modes, while later in the discharge ELMs are more likely to be triggered by peeling modes. The choice of the critical pressure gradient for a pressure-driven ballooning mode, the parameter related to the vacuum energy, and temperature at the separatrix all have an influence on the time evolution of ELMs, but they do not affect the global plasma confinement in the simulation results. The stability criteria used in the JETTO code are calibrated using the HELENA and MISHKA MHD stability codes.

In the simulations, a compound model is used for each ELM crash. The initial stage of each ELM crash is triggered either by a pressure-driven ballooning mode or by a current-driven peeling mode. After the initial stage, the continuation of the ELM crash is triggered by a current-driven peeling mode, which is made more unstable by the reduction in the pressure gradient during the initial stage of the crash. This compound ELM crash model reduces the pedestal current density just below the threshold for the peeling mode instability. In effect, the model provides an upper bound estimate for the pedestal current density that remains after an ELM crash. As the pedestal current density rebuilds after each ELM crash, the pressure gradient, which rebuilds faster than the current density, stabilizes the peeling mode. As the pedestal pressure gradient and current density rebuild between ELM crashes, there is a competition between the the ballooning modes and the peeling modes to determine which instability triggers the next ELM crash.

The accuracy of the simulations would be improved by a more detailed understanding of the nonlinear development of each ELM crash. For example, it is likely that magnetic reconnection layers remove current density from the pedestal during an ELM crash more rapidly than the relatively slow classical current diffusion used in the JETTO code. A more sophisticated ELM crash model is needed to compute the actual changes in the temperature, density, and current density during an ELM crash.

ACKNOWLEDGMENTS

T.O. acknowledges the Royal Thai Government and the Development and Promotion for Science and Technology Talents Project of Thailand (DPST) for their support. T.O. also thanks Dr. A. Pankin for his comments on this paper. This work was conducted partly under European Fusion Development Agreement. It was supported in part by the U.S. Department of Energy (DOE) under Contract No. DE-FG02-92-ER-5414, by the UK Department of Trade and Industry, and by EURATOM.

[1] J. W. Connor, H. R. Hastie, H. R. Wilson, and R. L. Miller, Phys. Plasmas **5**, 2687 (1998).
[2] J. Kinsey, T. Onjun, G. Bateman, A. H. Kritz, A. Pankin, G. M. Staebler, and R. E. Waltz, Nucl. Fusion **43**, 1845 (2003).
[3] R. Aymar, P. Barabaschi, and Y. Shimomura, Plasma Phys. Controlled Fusion **44**, 519 (2002).
[4] H. R. Wilson, J. W. Connor, A. R. Field, S. J. Fielding, R. L. Miller, L. L. Lao, J. R. Ferron, and A. D. Turnbull, Phys. Plasmas **6**, 1925 (1999).
[5] P. Gohil, Phys. Rev. Lett. **61**, 1603 (1988).
[6] G. T. A. Huysmans, T. C. Hender, and B. Alper, Nucl. Fusion **38**, 179 (1998).
[7] G. T. A. Huysmans, T. C. Hender, B. Alper *et al.*, Nucl. Fusion **39**, 1489 (1999).
[8] H. R. Wilson and R. L. Miller, Phys. Plasmas **6**, 873 (1999).
[9] J. Manickam, Phys. Fluids B **4**, 1901 (1992).
[10] J. S. Lonnroth, V. V. Parail, G. Corrigan *et al.*, Plasma Phys. Controlled Fusion **45**, 1689 (2003).
[11] V. V. Parail, G. Bateman, M. Becoulet *et al.*, Plasma Phys. Rep. **29**, 539 (2003).
[12] T. Onjun, A. H. Kritz, G. Bateman, V. Parail, J. Lonnroth, and G. Huysmans, Phys. Plasmas **11**, 3006 (2004).
[13] G. W. Pacher, H. D. Pacher, A. S. Kukushkin, G. Janeschitz, and G. Pereverzev, Nucl. Fusion **43**, 188 (2003).
[14] T. Onjun, A. H. Kritz, G. Bateman, V. Parail, H. Wilson, J. Lonnroth, G. Huysmans, and A. Dnestrovskij, Phys. Plasmas **11**, 1469 (2004).
[15] H. R. Wilson, J. W. Connor, A. R. Field, R. J. Hastie, R. L. Miller, and J. B. Taylor, Nucl. Fusion **40**, 713 (2000).
[16] P. B. Snyder, H. R. Wilson, J. R. F. L. L. Lao *et al.*, Phys. Plasmas **9**, 2037 (2002).
[17] A. B. Mikhailovskii, G. T. A. Huysmans, S. E. Sharapov, and W. Kerner, Plasma Phys. Rep. **23**, 844 (1997).
[18] G. Cenacchi and A. Taroni, JET-IR(88) **03** (1988).
[19] M. Erba, A. Cherubini, V. V. Parail, and A. Taroni, Plasma Phys. Controlled Fusion **39**, 261 (1997).
[20] W. A. Houlberg, K. C. Shaing, S. P. Hirshman, and M. C. Zarnstorff, Phys. Plasmas **4**, 3231 (1997).
[21] J. Stober, O. Gruber, A. Kallenbach *et al.*, Plasma Phys. Controlled Fusion **42**, A211 (2000).
[22] W. Suttrop, M. Kaufmann, H. J. de Blank *et al.*, Plasma Phys. Controlled Fusion **39**, 2051 (1997).
[23] L. D. Horton, J. P. Christiansen, J. Lingertat *et al.*, Plasma Phys. Controlled Fusion **41**, B329 (1999).
[24] A. M. Dimits, G. Bateman, M. A. Beer *et al.*, Phys. Plasmas **7**, 969 (2000).
[25] G. Saibene, L. D. Horton, R. Sartori, *et al.*, Nucl. Fusion **39**, 1133 (1999).